

Adaptive kinetic Monte Carlo simulation of methanol decomposition on Cu(100)

Lijun Xu,¹ Donghai Mei,² and Graeme Henkelman^{1,a)}¹*Department of Chemistry and Biochemistry, University of Texas at Austin, Austin, Texas 78712-0165, USA*²*Institute for Interfacial Catalysis, Pacific Northwest National Laboratory, Richland, Washington 99352, USA*

(Received 21 July 2009; accepted 10 December 2009; published online 31 December 2009)

The adaptive kinetic Monte Carlo method was used to calculate the decomposition dynamics of a methanol molecule on Cu(100) at room temperature over a time scale of minutes. Mechanisms of reaction were found using minimum mode following saddle point searches based on forces and energies from density functional theory. Rates of reaction were calculated with harmonic transition state theory. The dynamics followed a pathway from CH₃OH, CH₃O, CH₂O, HCO, and finally to CO. Our calculations confirm that methanol decomposition starts with breaking the O–H bond followed by breaking C–H bonds in the dehydrogenated intermediates until CO is produced. The bridge site on the Cu(100) surface is the active site for scissoring chemical bonds. Reaction intermediates are mobile on the surface which allows them to find this active reaction site. This study illustrates how the adaptive kinetic Monte Carlo method can model the dynamics of surface chemistry from first principles. © 2009 American Institute of Physics. [doi:10.1063/1.3281688]

I. INTRODUCTION

Determining the microscopic mechanisms of chemical reactions in nonideal systems is a very challenging problem. In heterogeneous catalysis, uncertainty about the active sites or reactive phases makes it difficult to establish correlations between structure and activity, let alone identify the possible intermediates and side reactions. Catalytic reactions on single crystal model surfaces are easier to study,^{1–3} but the overall microscopic mechanisms and kinetics are still difficult to determine with current experimental techniques. Theoretical studies are well suited for determining the mechanism of reactions, and provide a powerful tool when combined with experiments for validation of the reaction rates and products.^{4–8}

Transition state theory (TST) offers a framework for understanding the dynamics of systems where the important reactions are rare events. Long lived states correspond to minima on the potential (or free) energy surface (PES). These basins are separated by dividing surfaces of high free energy—the transition states. Rates of reaction are calculated within TST as the flux through the transition states.^{9,10} In solid- and gas-phase systems, atoms tend to vibrate around equilibrium positions so that stable states can be characterized by minima and transition states by saddle points on the PES. Under this approximation TST simplifies using a harmonic expansion of the potential about these critical points. Each reaction mechanism is described by a minimum energy pathway (MEP) and the transition state by the saddle point, which is a maximum along the MEP. The rate is evaluated as

$$k^{\text{hTST}} = \nu e^{-\Delta E/k_{\text{B}}T}, \quad (1)$$

where the barrier ΔE is the energy difference between the saddle point and the initial state

$$\Delta E = E^{\text{sp}} - E^{\text{init}}, \quad (2)$$

and ν is the reaction prefactor

$$\nu = \frac{\prod_{i=1}^N \nu_i^{\text{init}}}{\prod_{j=1}^{N-1} \nu_j^{\text{sp}}}, \quad (3)$$

which is the ratio of positive normal mode frequencies at the initial state and the saddle point.^{11,12}

If all possible reaction mechanisms and rates available to the system are known, kinetic Monte Carlo (KMC) can be used to simulate the reaction dynamics over long time scales.^{13–17} Typically though, the construction of a KMC model involves making significant approximations. The modeler must anticipate and calculate every accessible reactive event. In systems where accurate simulations over long time scales have been performed, including self-diffusion on metal surfaces,^{18,19} defect diffusion in oxides,²⁰ void filling in metals,²¹ and metal cluster diffusion on oxides,²² the dynamics reveal reaction mechanisms which were not anticipated and would not be included in a typical KMC event catalog.²³ Multiatom and long range events pose a significant problem for KMC because the possible number of such events grows rapidly with their extent. Another limitation of KMC is that in order to make a finite event table which includes all possible events, the simulation must be mapped onto a regular array or lattice so that structures can be matched to those in the event table. Off-lattice structures, defects, molecules assuming different conformations, solvent, and other nonideal effects are difficult to model with KMC.

^{a)}Electronic mail: henkelman@mail.utexas.edu.

A further challenge for modeling the dynamics of chemical reactions is that accurate empirical potentials are not generally available. Density functional theory (DFT) provides an acceptable accuracy for surface chemistry, but the cost is significant for computational methods which require sampling of the PES. For chemical systems where bond breaking is an activated process, harmonic TST makes the calculation of reaction rates from DFT tractable. When the initial and final states of a reaction are known, a MEP can be calculated using the nudged elastic band (NEB).^{24–26} A double ended approach such as the NEB works well for simple systems where a mix of trial and error and intuition is enough to find the most likely reaction geometries. For more complex systems, it becomes difficult to know *a priori* how the system will react. Then it is better to use a min-mode following method to search from an initial state minimum to find saddle points which lead to possibly unknown final states. This class of single ended methods iteratively finds the lowest curvature mode using a dimer,²⁷ Lagrange multiplier,²⁸ or the Lanczos method,²⁹ and then follows the mode up the potential while relaxing in all other directions until a saddle point is reached. Many searches with different initial conditions are needed to identify all the important saddles. This is more expensive than finding a single pathway to a known final state, but the information is more valuable, particularly when the system reacts in an unexpected way. The min-mode approach has been used to determine reaction mechanisms for metal clusters on oxides²² and small molecules on metal surfaces.^{30,31} If the important reaction mechanisms are identified and mapped onto a simulation grid, KMC can be used to model the Markov dynamics over very long times.^{15,17} When only a modest number of rates is important for capturing the dynamics and these are modeled accurately with DFT, agreement with experiment can be obtained.¹⁶

Very recently it has become possible to combine min-mode following saddle searches with DFT and use the reactions discovered directly with KMC in an adaptive KMC (aKMC) simulation.³² The method is described as adaptive because the event table is not fixed before the KMC simulation begins; instead it adapts to the structures followed in the dynamics.^{19,33}

In this work, we use the aKMC approach to study the decomposition dynamics of a methanol molecule on Cu(100). Methanol is an important industrial intermediate and feed stock used to produce other chemical products. Single crystals have been widely used in studying adsorption and reaction of methanol and its derivatives. Wachs and Madix studied the oxidation of methanol on Cu(110) with flash desorption spectroscopy and concluded that (1) methanol adsorbs weakly on Cu(110) and desorbs at room temperature, (2) methanol undergoes sequential dehydrogenations into methoxy and formaldehyde before oxidation, (3) reaction intermediates and products such as formaldehyde, water, and hydrogen are detected, and (4) clean Cu(110) is much less able to activate methanol than the oxygen precovered surface.³⁴ Similar results were reported by Sexton for adsorption and reaction on Cu(100) (Ref. 35) and by Russell *et al.* on Cu(111).³⁶ Numerous experiments using different techniques on both single crystals and Cu particles supported

on oxides confirm this mechanism.^{37–50} There is consensus that the mechanism of methanol decomposition on Cu involves first breaking the O–H bond before breaking C–H bonds, with the latter as the rate limiting step. However, experimental studies have not been clear on the role of oxygen in methanol activation. Theoretical calculations, especially DFT studies, can reveal detailed information on adsorption geometry and reaction energetics. Gomes *et al.*⁵¹ and Greeley and Mavrikakis⁵² used DFT to calculate the adsorption of methanol and the possible decomposition intermediates and products on Cu(111). They confirmed the weak adsorption of methanol and the strong binding of methoxy. Greeley *et al.* found that hydrogen abstraction from methoxy into formaldehyde on Cu(111) has a high barrier of 1.4 eV. Sakong and co-workers studied methanol oxidation on both clean and oxygen precovered Cu(110) and Cu(100) surfaces with DFT.^{53–56} They also found that the O–H bond breaking into methoxy was rapid while the sequential C–H bond breaking was slow with barriers of ~ 1.4 eV. They clarified that oxygen adatoms do not change the dehydrogenation barriers, instead, oxygen facilitates removal of the dissociated hydrogen adatoms by forming water, which rapidly desorbs. Since there is quite a bit known about the initial steps and intermediates of methanol decomposition on Cu(100), we used this as a system to see if an unbiased dynamics simulation reveal the same mechanisms of reaction as have been previously reported, and to demonstrate the effectiveness of the aKMC approach for studying surface chemistry.

II. METHODOLOGY

The aKMC method as applied in DFT simulations has been described in detail in Ref. 32. Here we briefly summarize the method and give the simulation parameters.

The aKMC simulation starts by searching for saddle points directly connected to the reactant state minimum on the PES. Saddle point searches were conducted with the min-mode following method using a dimer approach²⁷ with forward difference^{57,58} to identify the minimum mode. A distance of 0.01 Å separated the two images in the dimer. Each saddle point search was initiated by displacing the atoms in the adsorbate molecule by a random distance selected from a Gaussian distribution of width 0.1 Å. The reaction path from each unique saddle point was followed with a steepest descent trajectory to find the two connecting minima via that reaction path. These minimizations were initiated by displacing 0.1 Å forward and backward along the negative mode at the saddle. Only saddles with one connecting minimum corresponding to the reactant state were considered valid reaction pathways; the other minimum is the product state of the reaction. The event table was built using all such valid processes with barriers within $20k_B T$ of the lowest barrier process. Reaction prefactors were found using Eq. (3). The normal modes at the initial minimum and saddle point were calculated by diagonalizing Hessian matrices constructed by finite difference. Prefactors of reaction were found to lie in a standard range between 4×10^{12} and $5 \times 10^{15} \text{ s}^{-1}$, so that processes with the highest possible barrier in the event table occur with a probability of at most $e^{-20} 10^3 \approx 10^{-6}$ as com-

pared to the lowest barrier process. Higher barrier saddles were considered irrelevant because they would be selected with such a low probability in the dynamics.

Saddle point searches were repeated from each state until a sequence of ten valid saddles were found without finding a new process which would be added to the event table. If all saddles were found with equal probability, this stopping criterion corresponds to a 90% confidence that the event selected from the table of relevant saddles would be in the complete table.³² This assumption was tested for a step in the methanol decomposition dynamics with a significant number of valid processes within the $20k_B T$ window— CH_2O decomposition. With the criterion of ten sequential redundant searches, the most commonly found process was found seven times and the least was found two times. Using these values, the confidence is reduced from 90% to $1 - (1/10)(7/2) = 65\%$.³² When the number of redundant searches was increased to 20, no new processes were found and the most common process was found 15 times resulting in a confidence of $1 - (1/20)(2/15) = 63\%$. While our simulation confidence is not high enough to ensure that all processes have been found, it is high enough to reveal a likely reaction pathway. More searches would be better and will be possible in the future given the increasing amount of parallel computational resources available.

The selected event was chosen according to KMC with a probability proportional to its harmonic TST rate, from Eq. (1), and was made to occur by moving the system to the corresponding product state. The system clock was incremented by a time interval τ from the Poisson distribution of escape times

$$\tau = -\frac{\ln(\mu)}{\sum_i k_i^{\text{TST}}}, \quad (4)$$

where μ is a uniform random number between 0 and 1, and i ranges over all possible events. AKMC steps were repeated to model the state-to-state dynamics over a time scale set by the rate of transitions.

All energies and forces were calculated from DFT using the Vienna *ab initio* Simulation Package.⁵⁹ The Cu(100) surface was modeled by a three-layer, $p(3 \times 3)$ slab containing nine atoms per layer with the atoms in the bottom layer held frozen in bulk lattice positions. The Perdew–Wang 91 generalized gradient functional was used to model electronic exchange and correlation.⁶⁰ Vanderbilt pseudopotentials⁶¹ constructed within the projected augmented wave framework were used.⁶² A plane wave basis set with an energy cutoff of 274 eV and a $2 \times 2 \times 1$ k -point sampling of the Brillouin zone was found to be sufficient. Geometries were considered converged when the force dropped below 0.003 eV/Å on each atom.

The DFT parameters were chosen to be as relaxed as possible without corrupting the dynamical pathways. Optimizing computational efficiency reduced the overall cost of the simulation and allowed for a greater exploration of the energy landscape. The errors made in our calculation were tested by comparing the binding energy of methanol to Cu(100) calculated with the chosen parameters (0.4 eV) to more accurate settings. Increasing the k -point mesh to

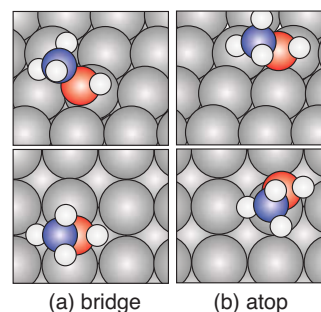


FIG. 1. The top and tilted views of a methanol molecule on Cu(100): (a) bridge and (b) atop site. Atom types from large to small circles are Cu (gray), O (red), C (blue), and H (white).

$3 \times 3 \times 1$, the vacuum gap between slabs by 4 Å, the cell size to $p(4 \times 4)$, and the plane wave cutoff to 400 eV, changed the binding energy by no more than 0.04 eV. This is within the uncertainty of the DFT functionals, and acceptable for understanding the qualitative mechanisms and time scales of reaction.

III. RESULTS

A. Methanol

Methanol adsorbs with the oxygen atom bonded directly with the Cu(100) surface, either at the bridge or atop site (see Fig. 1) with adsorption energies of 0.40 and 0.35 eV, respectively. This is in agreement with the experimental value of 0.43 eV.⁶³ The molecule is weakly bound to the surface so there may be other conformations with similar adsorption energies.⁵³

We started the simulation with the methanol molecule adsorbed over the bridge site. Saddle point searches found the possible reaction mechanisms illustrated in Fig. 2. The mechanisms can be categorized according to which bond breaks. O–H bond breaking produces a methoxy (CH_3O) group and a hydrogen atom on separate hollow sites (a). C–H bond breaking shows more complexity; the dissociated hydrogen can either adsorb on a hollow site (b and c), or bind with the oxygen atom to form another stable configuration of adsorbed methanol (f), or even release into the gas phase (h). C–O bond breaking results in adsorbed methyl and hydroxyl on bridge sites (e). There are also complicated processes which involve breaking and forming different types of bonds in a concerted way, a methane molecule can be extracted into gas phase by scissoring both C–O and O–H and forming a new C–H bond (d), and a gas-phase hydrogen molecule can be formed by breaking both O–H and C–H before forming a H–H bond (g). However, these concerted mechanisms have high barriers and are unlikely to occur at room temperature.

We also performed one aKMC step starting from the atop structure in Fig. 1(b) and found similar mechanisms for C–O and C–H bond breaking (see Fig. 3). The lowest energy O–H bond breaking event, however, is preferred at the bridge site.

We noticed that our searches did not identify a diffusion mechanism connecting the two states shown in Fig. 1. To better understand this, we did a separate NEB calculation between those two structures and found that there is no sig-

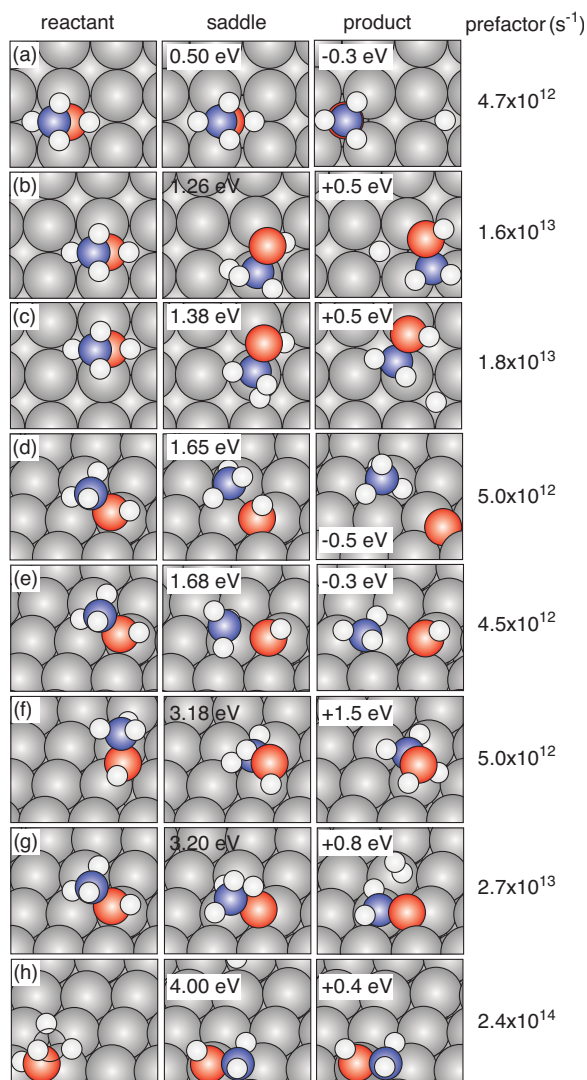


FIG. 2. Possible dissociation mechanisms of methanol are shown either from a top or tilted view. The energy of the saddle and product state is given relative to the initial state.

nificant transition barrier from the top site to the bridge site. The adsorption near the top site is a very shallow minimum and the diffusion saddle points are located extremely close to it, which made it hard to find using the settings of our search

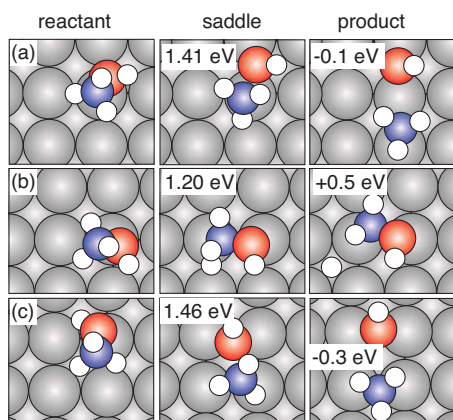


FIG. 3. Dissociation of a methanol molecule on the top site.

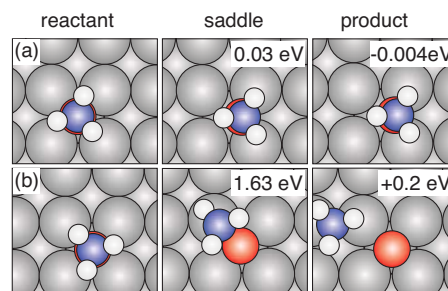


FIG. 4. Diffusion and dissociation of a methoxy group at the hollow site.

algorithm. Since diffusion and adsorption/readsorption processes do not change the initial state of the system, they were excluded from the event table.

Although methanol is not a complex molecule, we see a variety of possible dissociation mechanisms. O–H bond breaking [Fig. 2(a)] has the lowest barrier of 0.50 eV and a product with almost the highest stability. This is consistent with a previous study showing that methanol dissociation starts with O–H bond breaking over the bridge site on Cu(100).⁵³ Only at higher temperature would it be possible to see the extraction of a methane molecule to the gas phase [Fig. 2(d), which is also a mechanism for methane oxidation],⁶⁴ or the scissored methyl and hydroxyl groups on the surface [Fig. 2(e)].

The KMC selection of mechanism (a) in Fig. 2 occurred in 0.17 ms at room temperature and resulted in a new geometry with a methoxy group and hydrogen atom adsorbed at hollow sites. From this state, it is possible for the reverse process of methanol formation to occur with a barrier of 0.8 eV, but there is a much lower barrier of 0.2 eV for hydrogen diffusion. When mobile hydrogen atoms encounter each other, they can recombine forming H₂ with a barrier of 0.6 eV.⁵³ In our simulation, we assumed this desorption process for the isolated H atom and removed it from our simulation. Then we could focus on methoxy in the next step of our aKMC simulation.

B. CH₃O

The methoxy group binds at the hollow site on Cu(100) through its oxygen atom. Our simulation shows that methoxy can rapidly diffuse from the hollow site toward the adjacent bridge site with a tiny barrier of 0.03 eV [Fig. 4(a)]. The breaking of the C–O bond of methoxy on the hollow site has a high barrier of 1.63 eV [Fig. 4(b)]. No C–H bond breaking processes were found for methoxy starting from this hollow site. The fastest event at this step, which was selected in the aKMC simulation, is diffusion to the bridge site. This is consistent with previous work showing that methoxy reacts at bridge sites.⁵³

From the bridge site, the methoxy can either diffuse back to the hollow site [Fig. 5(a)] or one of the C–H bonds can break. The detached hydrogen atom via the CH bond scissoring might either stay on the surface (b, c, and d) or (with a high barrier) directly release into the gas phase (e). The diffusion barrier of methoxy is much lower than other mechanisms so that methoxy that bind at the bridge and hollow sites were considered to be in thermal equilibrium.³² The

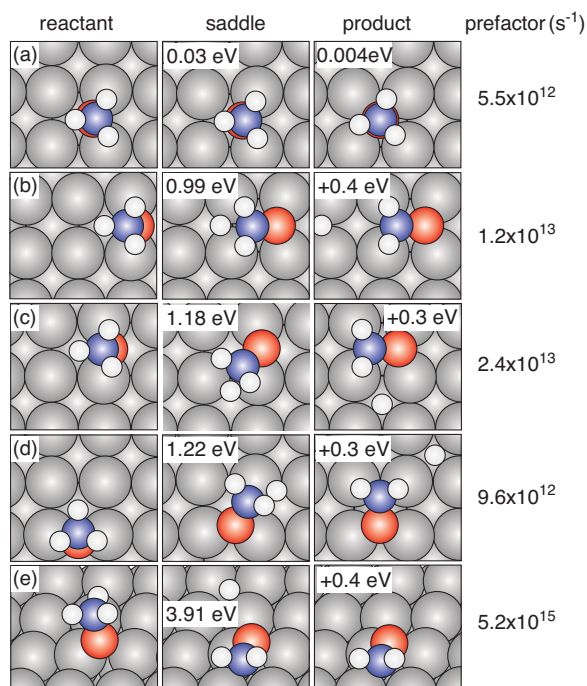


FIG. 5. Reaction mechanisms of a methoxy group at the bridge site.

aKMC simulation then chose an event which brought the system out from one of these two states, the C–H scissoring mechanism shown in Fig. 5(b), with a final state consisting of a hydrogen adatom and a formaldehyde (CH_2O) molecule. We also notice that our calculated methoxy decomposition barrier is 1.0 eV, which is consistent with previous work⁵³ but much lower than 1.71 eV calculated from a cluster model using the B3LYP functional.⁶⁵ The time for methoxy dissociation event was 228 s. This slow reaction time shows that methoxy activation should take place at higher temperatures.³⁴ As in the previous step, we removed the hydrogen atom from the system to leave formaldehyde. This is justified because the reverse barrier of 0.60 eV is much higher than the hydrogen diffusion barrier.

C. CH_2O

Formaldehyde adsorbs most favorably with both C and O atoms in direct contact with the Cu(100) surface,⁵³ which is also the geometry found in our kinetics. Formaldehyde can easily rotate and diffuse on the surface [Figs. 6(a)–6(e)] with barriers less than 0.5 eV. The aKMC algorithm considered the multiple formaldehyde adsorption states to be in equilibrium. The C–H bond breaking events (f–i) of formaldehyde generate a hydrogen atom at a neighboring hollow site and a formyl (HCO) group between two bridge sites. These events have barriers of ~ 0.9 eV; the chosen event occurred in 306 s, leaving a H adatom to diffuse away and an adsorbed HCO molecule.

D. HCO

Formyl species from the previous aKMC step adsorbs at the bridge sites with both C–Cu and O–Cu bonds. The C–H bond in HCO points away from the surface (Fig. 7). Saddle point searches found three types of reaction mechanisms.

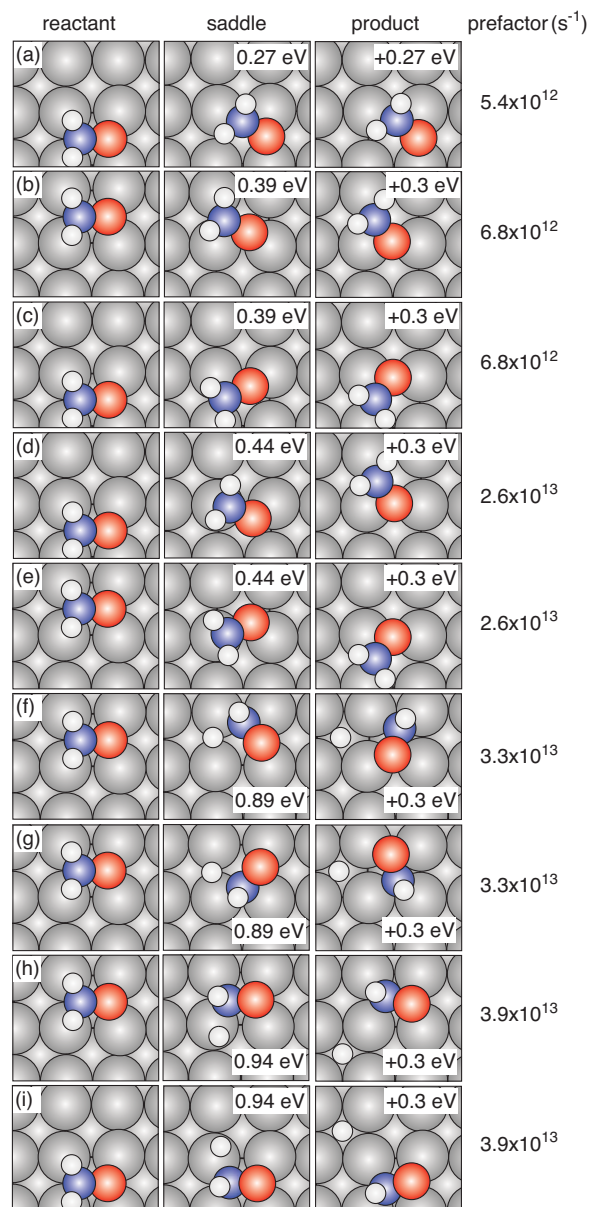


FIG. 6. Reaction mechanisms of a formaldehyde group on the bridge sites.

The C–H bond can break with a barrier of only 0.6 eV leaving an adsorbed hydrogen atom and a CO molecule bound to the surface [Figs. 7(a)–7(d)]. These C–H bond scissoring processes are exothermic, releasing 0.8 eV due to the strong binding of CO on Cu(100). Breaking the C–O bond (f) requires more energy (1.1 eV) and the products are not as stable as those from the C–H bond breaking. We also found an unphysical mechanism (e), which appears to result in formyl diffusion, but actually involves the diffusion of an entire row of Cu atoms. This is an artifact of our small system size and the process was removed from our event table. The aKMC algorithm chose the C–H bond breaking event in a simulation time of 0.3 ms, leaving an isolated CO molecule after removing the coadsorbed hydrogen atom.

E. CO

Figure 8 shows how the CO molecule can rapidly diffuse across the bridge site between two hollow sites with a low

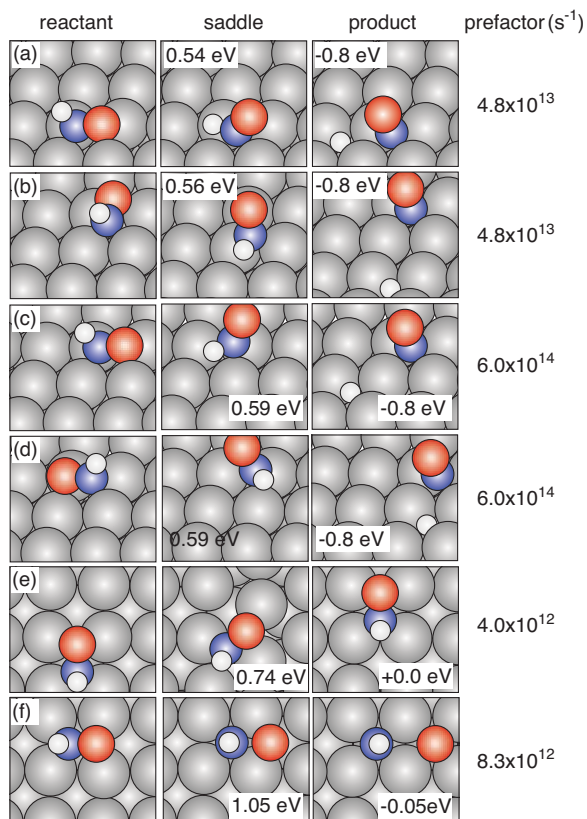


FIG. 7. Possible reactions of a formyl group at the bridge sites.

barrier of 0.29 eV or break the C–O bond with an energy of over 2.4 eV. At room temperature, the bond breaking event could not occur in an experimental time scale, so our methanol decomposition simulation ends with a CO molecule diffusing on the surface. Furthermore, the desorption energy of 1.7 eV is lower than the decomposition barrier so that decomposition would only take place at elevated pressures.

IV. DISCUSSION

Our simulations show that the initial activation of methanol on Cu(100) is through scissoring the O–H bond, followed by C–H bonds, and finally the C–O bond. Figure 9 summarizes the complete methanol decomposition path followed in our dynamics simulation.

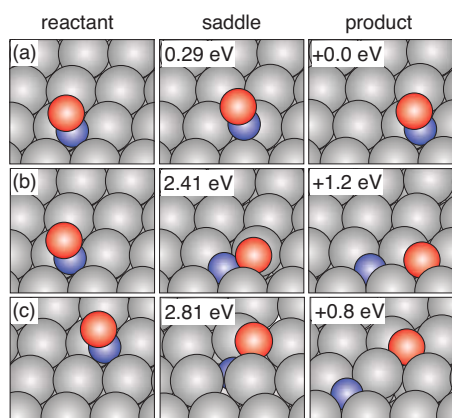


FIG. 8. Diffusion and dissociation of CO.

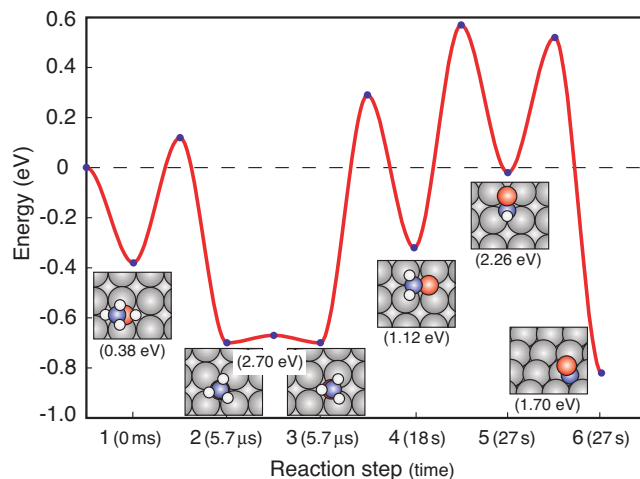


FIG. 9. The overall decomposition path for methanol on Cu(100). Note that the dissociated hydrogen adatoms are not shown in the insets. The zero of energy is aligned to the methanol molecule in gas phase, ignoring the energetics of desorbing H atoms. The adsorption energy for each species is given in parentheses.

At room temperature, methanol exhibits three types of motion on the surface: rotating and diffusing on the surface (<0.1 eV), desorbing into the gas phase (0.40 eV), and dissociating via the O–H bond breaking (0.50 eV). Dissociation is the least frequent event at room temperature, consistent with the weak chemical adsorption observed in experiments.³⁴ Once methanol dissociates into methoxy and a hydrogen adatom, the system energy drops due to strong adsorbate-surface bonding. After this step the decomposition continues via dehydrogenation. The detached H atoms bind strongly at hollow sites and are free to diffuse with a barrier of 0.2 eV. At reasonable coverages, two H adatoms can meet and recombine at room temperature, but this is a slow process. The associative desorption barrier for H₂ is 0.7 eV,^{66,67} which occurs on the time scale of seconds which is still faster than the dehydrogenation of methoxy. The assumption in our work is that hydrogen adatoms desorb, without interacting with intermediate species on the surface. In real experiments, the presence of hydrogen plays a significant role. H₂ adsorbs dissociatively on Cu(100) with a barrier of 0.6 eV (lower than desorption)⁶⁷ so that hydrogen is energetically favored on the surface and will be present at low temperature or when there is a significant partial pressure in the gas phase. Then, hydrogenation processes will compete with methanol decomposition, unless the hydrogen is removed, for example, in the form of water with an oxygen precovered surface.^{34,35} Since methoxy adsorbs strongly on the surface and its further dehydrogenation is difficult, methoxy is the dominant intermediate species, which is consistent with experimental observation.^{34,35} All subsequent products generated after the dissociation of methoxy in our simulation are mobile on the surface at room temperature, so that the formation of other products is possible.

With this case study, we demonstrated that the adaptive KMC simulation can automatically provide mechanisms of sequential chemical reactions. The dynamics follow molecules into active sites where the reactions take place. The method is able to find complex reaction and diffusion mechanisms.

Ideally the aKMC simulation would run automatically to follow the reaction dynamics, but this was not entirely possible in the simulation presented here. The cost of each step was significant so that we could not afford to model the diffusion events which would not lead to new products. By removing the dissociated H adatoms, we were able to focus on the interesting species and accelerate the simulation to follow the decomposition of methanol. The computational cost of these simulations is determined by the number of saddle point searches performed using forces from DFT. Fortunately these are independent and done in parallel on supercomputers. As larger and massively parallel computational resources become available in the future, larger first-principles based aKMC simulations will be possible.

V. CONCLUSION

By studying the decomposition of a methanol molecule on Cu(100), we have shown that the adaptive KMC can be used to study pathways of heterogeneous catalysis at the first principles level. A set of diffusion and reaction mechanisms were found for methanol and its subsequent dissociation intermediates which show the order of bond breaking and the active reaction sites for the decomposition. This formidable number of calculations is handled automatically and in parallel with job control and data analysis software.⁶⁸

ACKNOWLEDGMENTS

This work was supported by the National Science Foundation (Grant No. CHE-0645497) and the Robert A. Welch Foundation under Grant No. F-1601. D.M. was supported by a Laboratory Directed Research and Development (LDRD) project at Pacific Northwest National Laboratory (PNNL). The authors used the resources in the Texas Advanced Computing Center and computing time granted by the Science Theme Project (Grant No. ST25428) using the Molecular Science Computing Facility in the William R. Wiley Environmental Molecular Sciences Laboratory (EMSL), a U.S. Department of Energy national scientific user facility located at PNNL.

¹T. Engel and G. Ertl, *Adv. Catal.* **28**, 1 (1979).

²R. J. Behm, P. A. Thiel, P. R. Norton, and G. Ertl, *J. Chem. Phys.* **78**, 7437 (1983).

³P. L. J. Gunter, J. W. Niemantsverdriet, F. H. Ribeiro, and G. A. Somorjai, *Catal. Rev.-Sci. Eng.* **39**, 77 (1997).

⁴T. S. Askgaard, J. K. Nørskov, C. V. Ovesen, and P. Stoltze, *J. Catal.* **156**, 229 (1995).

⁵B. Uberuaga, M. Levskovar, A. P. Smith, H. Jónsson, and M. Olmstead, *Phys. Rev. Lett.* **84**, 2441 (2000).

⁶K. Judai, A. S. Worz, S. Abbet, J. M. Antonietti, U. Heiz, A. D. Vitto, L. Giordano, and G. Pacchioni, *Phys. Chem. Chem. Phys.* **7**, 955 (2005).

⁷K. Honkala, A. Hellman, I. N. Remediakis, A. Logadottir, A. Carlsson, S. Dahl, C. Christensen, and J. K. Nørskov, *Science* **307**, 555 (2005).

⁸M. P. Andersson, E. Abild-pedersen, I. N. Remediakis, T. Bligaard, G. Jones, J. Engbæk, O. Lytken, S. Hørch, J. H. Nielsen, J. Sehested, J. R. Rostrup-nielsen, J. K. Nørskov, and I. Chorkendorff, *J. Catal.* **255**, 6 (2008).

⁹H. Eyring, *J. Chem. Phys.* **3**, 107 (1935).

¹⁰E. Wigner, *Trans. Faraday Soc.* **34**, 29 (1938).

¹¹C. Wert and C. Zener, *Phys. Rev.* **76**, 1169 (1949).

¹²G. H. Vineyard, *J. Phys. Chem. Solids* **3**, 121 (1957).

¹³A. B. Bortz, M. H. Kalos, and J. L. Lebowitz, *J. Comput. Phys.* **17**, 10 (1975).

¹⁴D. T. Gillespie, *J. Comput. Phys.* **22**, 403 (1976).

¹⁵D. Mei, Q. Ge, M. Neurock, L. Kieken, and J. Lerou, *Mol. Phys.* **102**, 361 (2004).

¹⁶K. Reuter, D. Frenkel, and M. Scheffler, *Phys. Rev. Lett.* **93**, 116105 (2004).

¹⁷L. Xu, C. T. Campbell, H. Jónsson, and G. Henkelman, *Surf. Sci.* **601**, 3133 (2007).

¹⁸M. R. Sørensen and A. F. Voter, *J. Chem. Phys.* **112**, 9599 (2000).

¹⁹G. Henkelman and H. Jónsson, *Phys. Rev. Lett.* **90**, 116101 (2003).

²⁰B. P. Uberuaga, R. Smith, A. R. Cleave, F. Montalenti, G. Henkelman, R. W. Grimes, A. F. Voter, and K. E. Sickafus, *Phys. Rev. Lett.* **92**, 115505 (2004).

²¹B. P. Uberuaga, R. G. Hoagland, A. F. Voter, and S. M. Valone, *Phys. Rev. Lett.* **99**, 135501 (2007).

²²L. Xu, G. Henkelman, C. T. Campbell, and H. Jónsson, *Phys. Rev. Lett.* **95**, 146103 (2005).

²³A. F. Voter, F. Montalenti, and T. C. Germann, *Annu. Rev. Mater. Res.* **32**, 321 (2002).

²⁴H. Jónsson, G. Mills, and K. W. Jacobsen, in *Classical and Quantum Dynamics in Condensed Phase Simulations*, edited by B. J. Berne, G. Cicciotti, and D. F. Coker (World Scientific, Singapore, 1998), pp. 385–404.

²⁵G. Henkelman and H. Jónsson, *J. Chem. Phys.* **113**, 9978 (2000).

²⁶G. Henkelman, B. P. Uberuaga, and H. Jónsson, *J. Chem. Phys.* **113**, 9901 (2000).

²⁷G. Henkelman and H. Jónsson, *J. Chem. Phys.* **111**, 7010 (1999).

²⁸L. J. Munro and D. J. Wales, *Phys. Rev. B* **59**, 3969 (1999).

²⁹R. Malek and N. Mousseau, *Phys. Rev. E* **62**, 7723 (2000).

³⁰D. Mei, L. Xu, and G. Henkelman, *J. Catal.* **258**, 44 (2008).

³¹D. Mei, L. Xu, and G. Henkelman, *J. Phys. Chem. C* **113**, 4522 (2009).

³²L. Xu and G. Henkelman, *J. Chem. Phys.* **129**, 114104 (2008).

³³G. Henkelman and H. Jónsson, *J. Chem. Phys.* **115**, 9657 (2001).

³⁴I. Wachs and R. Madix, *J. Catal.* **53**, 208 (1978).

³⁵B. A. Sexton, *Surf. Sci.* **88**, 299 (1979).

³⁶J. J. N. Russell, S. Gates, and J. J. T. Yates, *Surf. Sci.* **163**, 516 (1985).

³⁷R. Ryberg, *Phys. Rev. Lett.* **49**, 1579 (1982).

³⁸R. Ryberg, *J. Electron Spectrosc. Relat. Phenom.* **29**, 59 (1983).

³⁹R. Ryberg, *J. Chem. Phys.* **82**, 567 (1985).

⁴⁰A. Peremans, F. Maseri, J. Darville, and J. M. Gilles, *J. Vac. Sci. Technol. A* **8**, 3224 (1990).

⁴¹X. D. Jiang, J. E. Parmeter, C. A. Estrada, and D. W. Goodman, *Surf. Sci.* **249**, 44 (1991).

⁴²D. B. Clarke, D. K. Lee, M. J. Sandoval, and A. T. Bell, *J. Catal.* **150**, 81 (1994).

⁴³T. H. Ellis and H. Wang, *Langmuir* **10**, 4083 (1994).

⁴⁴L. Domokos, T. Katona, and A. Molnar, *Catal. Lett.* **40**, 215 (1996).

⁴⁵J. P. Camplin and E. M. Mccash, *Surf. Sci.* **360**, 229 (1996).

⁴⁶Z. M. Hu, K. Takahashi, and H. Nakatsuji, *Surf. Sci.* **442**, 90 (1999).

⁴⁷M. A. Karolewski and R. G. Cavell, *Appl. Surf. Sci.* **173**, 151 (2001).

⁴⁸K. Mudalige and M. Trenary, *J. Phys. Chem. B* **105**, 3823 (2001).

⁴⁹C. Ammon, A. Bayer, G. Held, B. Richter, T. Schmidt, and H. P. Steinruck, *Surf. Sci.* **507-510**, 845 (2002).

⁵⁰S. Polmann, A. Bayer, C. Ammon, and H. P. Steinruck, *Z. Phys. Chem.* **218**, 957 (2004).

⁵¹J. R. B. Gomes and J. A. N. F. Gomes, *Surf. Sci.* **471**, 59 (2001).

⁵²J. Greeley and M. Mavrikakis, *J. Catal.* **208**, 291 (2002).

⁵³S. Sakong and A. Gross, *J. Catal.* **231**, 420 (2005).

⁵⁴S. Sakong, C. Sendner, and A. Gross, *J. Mol. Struct.: THEOCHEM* **771**, 117 (2006).

⁵⁵C. Sendner, S. Sakong, and A. Gross, *Surf. Sci.* **600**, 3258 (2006).

⁵⁶S. Sakong and A. Gross, *J. Phys. Chem. A* **111**, 8814 (2007).

⁵⁷R. A. Olsen, G. J. Kroes, G. Henkelman, A. Arnaldsson, and H. Jónsson, *J. Chem. Phys.* **121**, 9776 (2004).

⁵⁸A. Heyden, A. T. Bell, and F. J. Keil, *J. Chem. Phys.* **123**, 224101 (2005).

⁵⁹G. Kresse and J. Hafner, *Phys. Rev. B* **47**, 558 (1993).

⁶⁰J. P. Perdew, in *Electronic Structure of Solids*, edited by P. Ziesche and H. Eschrig (Akademie, Berlin, 1991), pp. 11–20.

⁶¹D. Vanderbilt, *Phys. Rev. B* **41**, 7892 (1990).

⁶²G. Kresse and J. Joubert, *Phys. Rev. B* **59**, 1758 (1999).

⁶³B. A. Sexton and A. E. Hughes, *Surf. Sci.* **140**, 227 (1984).

⁶⁴G. Fratesi, P. Gava, and S. D. Gironcoli, *J. Phys. Chem. C* **111**, 17015 (2007).

⁶⁵M. A. N. Santiago, M. A. Sanchez-castillo, R. D. Cortright, and J. A. Dumesic, *J. Catal.* **193**, 16 (2000).

⁶⁶B. Hammer, M. Scheffler, K. W. Jacobsen, and J. K. Nørskov, *Phys. Rev. Lett.* **73**, 1400 (1994).

⁶⁷P. Kratzer, B. Hammer, and J. K. Nørskov, *Surf. Sci.* **359**, 45 (1996).

⁶⁸Available at <http://theory.cm.utexas.edu/vtsttools/>.